Dysregulation of myelin synthesis and actomyosin function underlies aberrant myelin in CMT4B1 neuropathy

Marta Guerrero-Valero[a], Federica Grandi[a], Silvia Cipriani[a], Valeria Alberizzi[a], Roberta Di Guardo[a], Gaetan Chicanne[b], Linda Sawade[c], Francesca Bianchi[d], Ubaldo Del Carro[d], Ivan De Curtis[e], Davide Pareyson[f], Yesim Parman[g], Angelo Schenone[h], Volker Haucke[c], Bernard Payrastre[b], and Alessandra Bolino[a,1]

[a]Human Inherited Neuropathies Unit, Institute of Experimental Neurology (INSPE) and Division of Neuroscience, Istituto di Ricovero e Cura a Carattere Scientifico (IRCCS) Ospedale San Raffaele, 20132 Milan, Italy; [b]Inserm UMR-1048, I2MC, Université Toulouse 3 Paul Sabatier, 31432 Toulouse, France; [c]Department of Molecular Pharmacology and Cell Biology, Leibniz-Forschungsinstitut für Molekulare Pharmakologie, 13125 Berlin, Germany; [d]Department of Neurology, IRCCS Ospedale San Raffaele, 20132 Milan, Italy; [e]Cell Adhesion Unit, Division of Neuroscience, IRCCS Ospedale San Raffaele, 20132 Milan, Italy; [f]Unit of Rare Neurodegenerative and Neurometabolic Diseases, Department of Clinical Neurosciences, Fondazione IRCCS Istituto Neurologico Carlo Besta, 20133 Milan, Italy; [g]Istanbul Faculty of Medicine, Neurology Department, Istanbul University, 34390 Istanbul, Turkey; and [h]Department of Neurosciences, Rehabilitation, Ophthalmology, Genetic and Maternal Infantile Sciences, IRCCS Policlinico San Martino, University of Genoa, 16132 Genoa, Italy

Edited by Mikael Simons, TU Munich, Munich, Germany, and accepted by Editorial Board Member Stephen T. Warren January 25, 2021 (received for review May 13, 2020)

Charcot-Marie-Tooth type 4B1 (CMT4B1) is a severe autosomal recessive demyelinating neuropathy with childhood onset, caused by loss-of-function mutations in the myotubularin-related 2 (*MTMR2*) gene. MTMR2 is a ubiquitously expressed catalytically active 3-phosphatase, which in vitro dephosphorylates the 3-phosphoinositides PtdIns3*P* and PtdIns(3,5)P_2, with a preference for PtdIns(3,5)P_2. A hallmark of CMT4B1 neuropathy are redundant loops of myelin in the nerve termed myelin outfoldings, which can be considered the consequence of altered growth of myelinated fibers during postnatal development. How MTMR2 loss and the resulting imbalance of 3′-phosphoinositides cause CMT4B1 is unknown. Here we show that MTMR2 by regulating PtdIns(3,5)P_2 levels coordinates mTORC1-dependent myelin synthesis and RhoA/myosin II-dependent cytoskeletal dynamics to promote myelin membrane expansion and longitudinal myelin growth. Consistent with this, pharmacological inhibition of PtdIns(3,5)P_2 synthesis or mTORC1/RhoA signaling ameliorates CMT4B1 phenotypes. Our data reveal a crucial role for MTMR2-regulated lipid turnover to titrate mTORC1 and RhoA signaling thereby controlling myelin growth.

Charcot-Marie-Tooth neuropathies | myelin | Schwann cells | phosphoinositides | myotubularin

Charcot-Marie-Tooth (CMT) neuropathies represent a broad group of disorders with a prevalence of 1 in 2,500 individuals (1–3). CMTs are generally characterized by progressive muscular atrophy and weakness, with an age at onset usually between the first and the second decades of life. Although demyelinating, axonal, or intermediate types are distinguished on the basis of the primary event of the disease, axonal loss or dysfunction usually correlates with functional impairment.

Among CMT neuropathies, CMT4B is a severe autosomal recessive demyelinating disease with childhood onset characterized by the presence of redundant loops of myelin in the nerve termed myelin outfoldings (4). CMT4B comprises three distinct genetic and clinical subtypes named CMT4B1, B2, and B3 (5). While CMT4B1 and B2 present with a classical motor and sensory neuropathy phenotype, CMT4B3-associated phenotypes range from a pure demyelinating polyneuropathy to an axonal neuropathy plus complex central nervous system (CNS) phenotypes. CMT4B neuropathies are caused by loss-of-function mutations in the myotubularin-related 2 (*MTMR2*, CMT4B1), *MTMR13* (also known as *SBF2*, SET binding factor 2, CMT4B2), and *MTMR5* (also known as *SBF1*, CMT4B3) genes (5–9). MTMR2, MTMR5, and MTMR13 belong to a broad family of protein tyrosine phosphatase/dual specificity-like phosphatases (PTP/DSP), which consists of 14 members in mammals (10). Six MTMRs are catalytically inactive, whereas eight are catalytically active enzymes, which dephosphorylate 3-phosphoinositides (PIs) (10, 11). PIs are potent signaling molecules that govern a variety of cellular functions, including cytoskeleton remodeling and membrane trafficking (12), key processes in myelinating glia in both the peripheral nervous system (PNS) and the CNS. Interestingly, among CMT4B-associated MTMRs, MTMR5 and MTMR13 are catalytically inactive proteins, whereas MTMR2 is a catalytically active enzyme, which in vitro is predicted to dephosphorylate the 3-phosphoinositides PtdIns3*P* and PtdIns(3,5)P_2 in the 3-position of the inositol ring (10, 13–15). Heterodimers of MTMR2 with either MTMR5 or MTMR13 are thought to possess higher enzymatic activity and a different subcellular localization as compared to MTMR2 homodimers (11, 16, 17).

Significance

Charcot-Marie-Tooth type 4B1 (CMT4B1) is a very severe demyelinating neuropathy with childhood onset, characterized by myelin outfoldings, a pathological aberrant form of myelination. This morphology may be the consequence of an excessive longitudinal growth of the myelinated internode during postnatal nerve development. We first demonstrated that loss of MTMR2 (Myotubularin-related 2) phosphatase causes CMT4B1. MTMR2 dephosphorylates phospholipids, important regulators of membrane trafficking, which is a key process in Schwann cells, the myelinating cells in the PNS. However, why loss of MTMR2 provokes CMT4B1 remains to be assessed. Here we propose a mechanism by which MTMR2, by regulating PtdIns(3,5)P_2 phosphoinositide levels, coordinates myelin synthesis and RhoA/myosin II-dependent cytoskeletal dynamics necessary to expand the membrane and promote myelin growth.

Author contributions: A.B. designed research; M.G.-V., F.G., S.C., V.A., R.D.G., G.C., L.S., and F.B. performed research; M.G.-V., F.G., S.C., G.C., F.B., U.D.C., I.d.C., V.H., B.P., and A.B. analyzed data; A.B. wrote the paper; and D.P., Y.P., and A.S. provided patient material.

The authors declare no competing interest.

This article is a PNAS Direct Submission. M.S. is a guest editor invited by the Editorial Board.

[1]To whom correspondence may be addressed. Email: bolino.alessandra@hsr.it.

This article contains supporting information online at https://www.pnas.org/lookup/suppl/doi:10.1073/pnas.2009469118/-/DCSupplemental.

Published March 2, 2021.

Using in vivo and ex vivo models of MTMR2 loss, we previously reported that PtdIns(3,5)P_2 is the preferential substrate of MTMR2 and that strategies aimed at rebalancing PtdIns(3,5)P_2 levels may be beneficial for CMT4B1 (18). However, why elevated levels of PtdIns(3,5)P_2 in the nerve specifically result in dysmyelination with myelin outfoldings, despite its importance for the development of future therapies, remains poorly understood.

Recent data suggest that the Ras-related GTPase Rab35 binds and recruits MTMR13/MTMR2 to down-regulate PtdIns(3,5)P_2-mediated mTORC1 activation and, thereby regulate myelin biogenesis (19). Here we show that not only mTORC1 but also RhoA-myosin II pathways are dysregulated specifically in CMT4B1 models as a consequence of PtdIns(3,5)P_2 elevation. We thus propose a mechanism by which lipid-mediated cytoskeleton remodeling and myelin synthesis control myelin growth at sites of membrane remodeling in the nerve.

Results

Increased PtdIns(3,5)P_2 Levels in Schwann Cells (SCs) Result in Myelin Oufoldings. MTMR2 is a ubiquitously expressed enzyme with a predicted 3-phosphatase activity toward both PtdIns3*P* and PtdIns(3,5)P_2 (Fig. 1*A*) (10, 13–15). We recently reported that PtdIns(3,5)P_2 levels are increased in fibroblasts and in Schwann cell/dorsal root ganglia (DRG) neuron coculture organotypic explants established from *Mtmr2* knockout (KO) mice (18). To probe MTMR2 function in humans, we measured PI levels from primary fibroblasts of three CMT4B1 patients, carrying homozygous loss-of-function or missense mutations in the *MTMR2* gene (p.T228fs*46; p.Q482*; p.L448P) (5). We found that PtdIns(3,5)P_2 levels were significantly elevated in patient cells, whereas PtdIns3*P* was only modestly increased (Fig. 1*B*). These findings further suggest that PtdIns(3,5)P_2 is the major physiological substrate of MTMR2 and that loss of MTMR2/Mtmr2 results in PtdIns(3,5)P_2 lipid level elevation. Consistent with this, we reported earlier that inhibition of the PIKfyve kinase, which generates PtdIns(3,5)P_2, could be an effective strategy to ameliorate CMT4B1 phenotype by lowering and rebalancing the levels of PtdIns(3,5)P_2 (18). Interestingly, apilimod (also known as STA-5326) is a recently identified small molecule compound, which specifically inhibits PIKfyve kinase activity (20). To explore whether apilimod-mediated PIKfyve inhibition could ameliorate CMT4B1, we treated Schwann cell/DRG neuron coculture organotypic explants established from *Mtmr2* KO embryos at embryonic day 13.5 (E13.5) using apilimod (at 300 nM). Of note, Mbp-positive myelin-forming fibers in *Mtmr2* KO coculture explants reproduce myelin outfoldings, as assessed by confocal microscopy and ultrastructural analysis (21, 22). These aberrant myelinated fibers, which are not observed in wild-type cocultures, are caused by Mtmr2 loss, as replacement of Mtmr2 by means of lentiviral vector transduction almost fully rescues this phenotype (21). We found that the fraction of Mbp-positive segments carrying myelin outfoldings in relation to the total number of Mbp-positive fibers was significantly reduced in apilimod-treated *Mtmr2* KO cultures compared to DMSO-treated cultures (Fig. 2 *A* and *B′*). In contrast, compound 19 (at 2.5 μM), a known inhibitor of PIK3CA (class III), the major kinase that produces PtdIns3*P* (23), was unable to ameliorate myelin outfoldings in *Mtmr2* KO Schwann cell/DRG neuron coculture explants (Fig. 2 *C*–*E′*).

These findings, along with previous data, strongly support the conclusion that elevated levels of PtdIns(3,5)P_2, but likely not of PtdIns3*P*, are associated with myelin outfoldings in Schwann cells in the nerve.

Enhanced mTORC1 Signaling in *Mtmr2* KO Models. PtdIns(3,5)P_2, as other signaling lipids, acts via binding to effector proteins at subcellular membranes (12, 24, 25). Recent data from nonmyelin-forming cells suggest that PtdIns(3,5)P_2 can drive mTORC1 activation at late

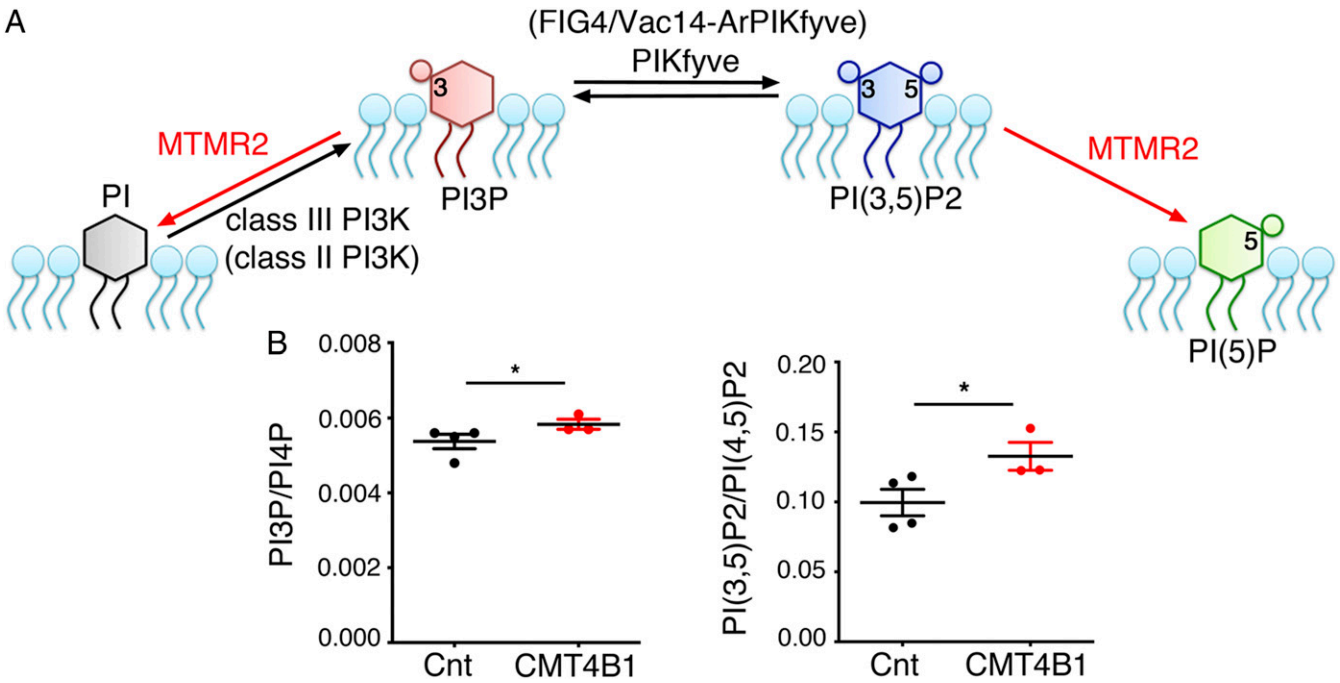

Fig. 1. Loss of MTMR2 leads to increased PtdIns(3,5)P_2 levels in CMT4B1 patient cells. (*A*) Predicted MTMR2 3′-phosphatase activity toward PtdIns3*P* (PI3P) and PtdIns(3,5)P_2 (PI3,5P_2). PIKfyve is the kinase which generates PtdIns(3,5)P_2. PtdIns3*P* at endosomes is primarily generated by class III PI3K, also with a possible contribution of class II PI3K (in parenthesis). In mammals, FIG4, in complex with other adaptor proteins such as Vac14/ArPIKfyve, potentiates PIKfyve activity to produce PtdIns(3,5)P_2. (*B*) PtdIns(3,5)P_2 levels [normalized to PtdIns(4,5)P_2] were significantly elevated in CMT4B1 patient fibroblasts as compared to age-matched controls, control (Cnt) 0.0995 ± 0.011, $n = 4$ and CMT4B1 0.1326 ± 0.01, $n = 3$, one-tailed Mann–Whitney *U* test, *$P = 0.029$, whereas PtdIns3*P* (normalized to PtdIns4*P*) Cnt 0.0054 ± 0.0002, $n = 4$ and CMT4B1 0.0058 ± 0.00012, $n = 3$ was modestly increased (one-tailed Mann–Whitney *U* test, *$P = 0.0238$). Representative of two independent experiments.

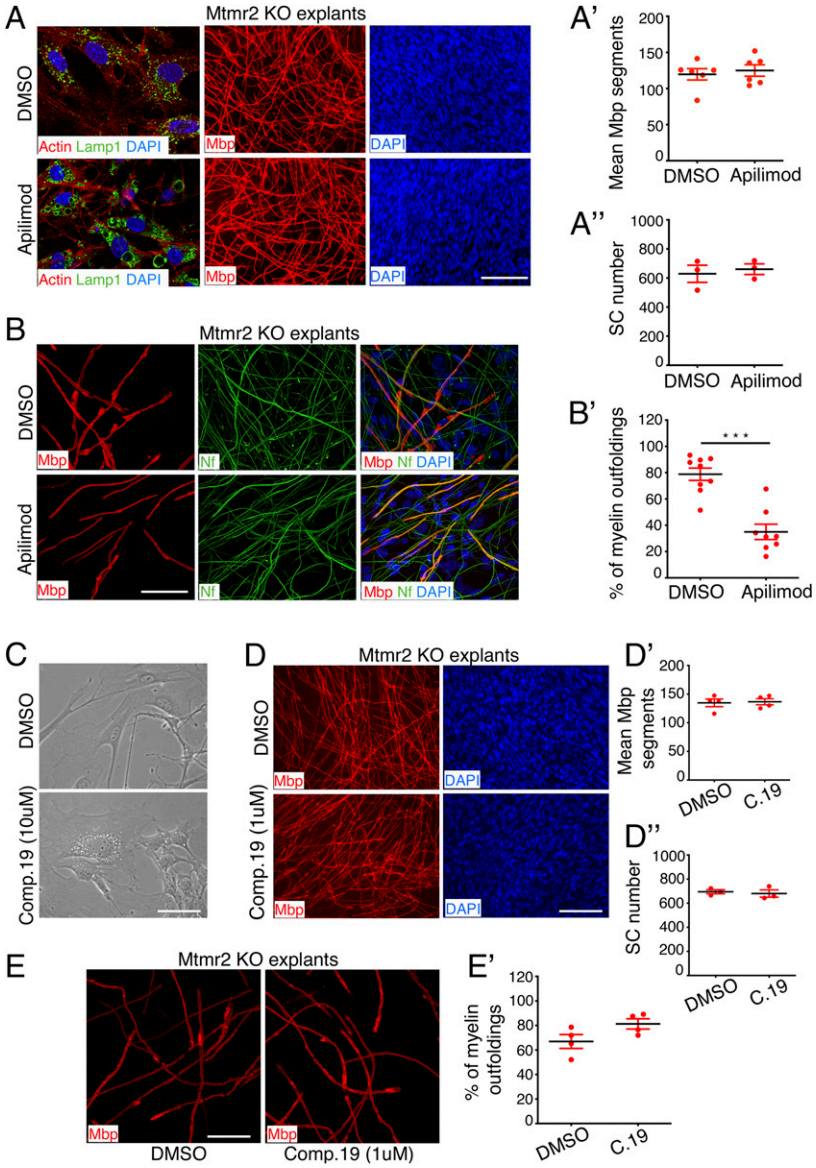

Fig. 2. Inhibition of PIKfyve but not of PI3K (Vps34) ameliorates myelin outfoldings in *Mtmr2* KO Schwann cell/DRG neuron coculture explants. (*A*) Representative fluorescence microscopy images of *Mtmr2* KO Schwann cell/DRG neuron coculture explants treated every other day for 14 d using 300 nM apilimod, which is the highest dose that does not interfere with myelination, as assessed by measuring the number of Mbp-positive segments and Schwann cell nuclei and quantified in *A′* and *A′′*, respectively. Mbp-positive segments: $n = 6$ DRG/coverslips DMSO-treated and $n = 6$ DRG/coverslips apilimod-treated, two-tailed Mann–Whitney *U* test, $P = 0.937$. Schwann cell nuclei, $n = 3$ DRG/coverslips DMSO-treated and $n = 3$ apilimod-treated, two-tailed Mann–Whitney *U* test, $P = 0.700$. On the *Left*, representative images of the costaining of Lamp1 and Phalloidin (F-actin) after 3 d of ascorbic acid treatment in differentiating conditions and following 90 min of apilimod treatment qualitatively demonstrate efficacy of PIKfyve inhibition. Enlargement of the Lamp1-positive late endosome/lysosomal compartment was observed, which is a well-established readout of PIKfyve inhibition and of decreased PtdIns(3,5)P_2 levels (20). (*B*) Representative confocal microscopy images of *Mtmr2* KO Schwann cell/DRG neuron coculture explants with myelin outfoldings treated every other day using 300 nM apilimod for 14 d in differentiating conditions. Apilimod reduces the percentage of Mbp-positive fibers carrying myelin outfoldings on the total number of Mbp-positive fibers, as quantified in B′, $n = 9$ DRG/coverslips DMSO-treated, 325 fibers analyzed and $n = 8$ DRG/coverslips apilimod-treated, 296 fibers analyzed, two-tailed Mann–Whitney *U* test, $***P = 0.0003$. Representative results from three independent experiments. (*C*) Representative bright-field images of cocultures treated using compound 19 (PI3K-VPS34 inhibitor 1) at 10 μM for 3 h qualitatively show efficacy of PI3K-Vps34 inhibition. Vacuolization-enlargement of endosomal compartments in a fibroblast as well as in Schwann cells can be observed, which is a well-established readout of PI3K inhibition. (*D*) Compound 19 treatment of *Mtmr2* KO Schwann cell/DRG neuron coculture explants every other day for 14 d in differentiating conditions does not interfere with myelination as indicated by similar numbers of Mbp-positive fibers and Schwann cell nuclei between DMSO- and compound 19-treated cultures, and quantified in *D′* and *D′′*, respectively. Mbp-positive segments: $n = 4$ DRG/coverslips DMSO-treated and $n = 4$ DRG/coverslips compound 19-treated, two-tailed Mann–Whitney *U* test, $P > 0.9999$. Schwann cell nuclei, $n = 3$ DRG/coverslips DMSO-treated and $n = 3$ compound19-treated, two-tailed Mann–Whitney *U* test, $P = 0.700$. (*E*) The percentage of Mbp-positive fibers carrying myelin outfoldings on the total number of Mbp-positive fibers in *Mtmr2* KO Schwann cell/DRG neuron coculture explants were not reduced by compound 19 treatment, as quantified in *E′* and displayed in confocal microscope representative images, $n = 4$ DRG/coverslips DMSO-treated, 207 fibers analyzed, and $n = 4$ DRG/coverslips compound 19-treated, 203 fibers analyzed, two-tailed Mann–Whitney *U* test, $P = 0.1143$. Results are mean ± SEM. Mbp, myelin basic protein, which stains myelinated segments; Nf, neurofilament, which stains axons and neurites. DAPI-positive nuclei are from Schwann cells, as DRG neurons are not dissociated and the cell bodies remain at the center of the organotypic explants, where myelination is not quantified. (Scale bar in *A*, 26 μm for LAMP1 staining and 116 μm for Mbp and DAPI staining; in *B*, 46 μm; in *C*, 64 μm; in *D*, 112 μm, and in *E*, 39 μm.)

endosomes and lysosomes (25, 26). Of note, constitutive mTORC1 activation in Schwann cells causes aberrant myelin (27–29). Consistent with these data, we recently reported that loss of the GTPase Rab35, which activates the MTMR13/MTMR2 complex, results in PtdIns(3,5)P_2-mediated mTORC1 overactivation and aberrant myelin (19). Here, we further corroborated these data by specifically investigating *Mtmr2* KO models with myelin outfoldings, in which PtdIns(3,5)P_2 levels are increased. We found that phosphorylation of S6, a downstream target of mTORC1, was significantly increased in *Mtmr2* KO sciatic nerves at P20 (*SI Appendix*, Fig. S1 *A* and *A′*) and in *Mtmr2* KO Schwann cell/DRG neuron coculture explants (*SI Appendix*, Fig. S1*C*) that suffer from elevated levels of PtdIns(3,5)P_2 (18). Rapamycin, a known mTORC1 inhibitor, reduced the fraction of Mbp-positive fibers with myelin outfoldings in *Mtmr2* KO Schwann cell/DRG neuron coculture explants (*SI Appendix*, Fig. S1 *D* and *D′*). Of note, rapamycin did not interfere with myelination under these conditions, as assessed by measuring the number of Mbp-positive segments and Schwann cell nuclei in *Mtmr2* KO Schwann cell/DRG neuron coculture explants (*SI Appendix*, Fig. S1 *B* and *B″*).

These data suggest that elevated mTORC1 activity contributes to aberrant myelin in *Mtmr2* KO models.

***Mtmr2* KO Nerves Display Altered Localization of Noncompact Myelin Proteins.** In myelinated fibers, tomacula and myelin outfoldings represent pathological focal myelin thickening or misfolding, respectively. Tomacula have been found to be predominantly associated with enhanced PI3K-Akt-mTORC1 pathway activity (30, 31). However, myelinated fibers carrying myelin outfoldings display normal myelin thickness (32–34), thus suggesting that the activation of the mTORC1 signaling in *Mtmr2* KO nerves may be locally restricted. Of note, in CMT4B mouse models, myelin outfoldings preferentially arise at paranodes and Schmidt–Lanterman incisures (SLIs) (32–36), which are local points of myelin remodeling and elongation formed by autotypic tight, adherens, and gap junctions (37, 38). We therefore hypothesized that myelin outfoldings in *Mtmr2* KO nerves may arise as a consequence of dysregulated myelin synthesis specifically occurring at these sites. Immunofluorescence analysis of teased fibers prepared from sciatic nerves at P20, showed that phosphorylated S6 mainly localized to the perinuclear region of Schwann cells where cytoplasm and organelles such as late endosomes and lysosomes are particularly enriched (*SI Appendix*, Fig. S1*E*), in the abaxonal region (*SI Appendix*, Fig. S1*E′*), and in the paranodes (*SI Appendix*, Fig. S1*E″*). Along the internode, the abaxonal localization became more prominent at P60, also surrounding SLIs (*SI Appendix*, Fig. S1 *F* and *F′*), in both control and *Mtmr2* KO nerves (*SI Appendix*, Fig. S1*G″*). When we examined *Mtmr2* KO fibers with aberrant myelin detected by phalloidin staining, we observed that phosphorylated S6 partially colocalized with aberrant myelin structures at paranodes (*SI Appendix*, Fig. S1 *G* and *G′*). Collectively, these data support the hypothesis that activation of mTORC1 is locally restricted at noncompact myelin regions from where myelin outfoldings preferentially arise.

Interestingly, we previously reported that both expression levels and localization of MAG (myelin-associated glycoprotein) and Dlg1 (Discs Large 1), two components of noncompact myelin regions, were altered in *Mtmr2* KO nerves at P60 (36). We therefore evaluated the expression and/or localization of molecular components of tight (claudin 5 and ZO-1) and adherens junctions (E-cadherin and p120 catenin), which form noncompact myelin in myelinated fibers (38–40). We found that the expression level of the transmembrane protein claudin 5 was decreased in total nerve lysates from *Mtmr2* KO nerves at P10 and P30 (Fig. 3*A* and *SI Appendix*, Fig. S2 *A–C*, *G*, and *H*) as well as in lysates prepared from membrane fractions of *Mtmr2* KO nerves at P30 (Fig. 3*A′* and *SI Appendix*, Fig. S3 *A–D′*). Consistent with this, we also observed that the localization but not the expression level of the cytosolic scaffold ZO-1, which is known to bind claudin 5, was altered at Schmidt–Lanterman incisures of *Mtmr2* KO nerves at P60 (Fig. 3 *B*, *D–E* and *SI Appendix*, Fig. S2 *A*, *B*, *D*, *F*, and *H′*). In contrast, the expression level and localization of both E-cadherin and p120 catenin were similar between *Mtmr2* KO and control nerves (35) (Fig. 3 *A*, *A′*, and *C* and *SI Appendix*, Fig. S2 *A–E* and *G*).

Altogether, these data suggest that expression level or localization of molecular components of noncompact myelin regions from where myelin outfoldings arise are altered in *Mtmr2* KO nerves. However, the general architecture of these regions as well as the assembly of tight and adherens junctions are preserved in mutant nerves (32, 35) (Fig. 3 *D* and *E*).

Enhanced RhoA-Myosin II Pathway in *Mtmr2* KO Nerves. Junction formation and maintenance is regulated by the actomyosin cytoskeleton (41–43). Moreover, impaired actin dynamics have been suggested to play a role in the generation of myelin misfoldings or outfoldings in several models (30, 44–50). We thus investigated the actomyosin cytoskeleton in *Mtmr2* KO nerves. Immunoblot analysis of sciatic nerve lysates showed that total actin protein levels were similar between mutant and control nerves (Fig. 3*F* and *SI Appendix*, Figs. S2 *A* and *B* and S3 *E* and *E′*). To assess the ratio between monomeric G-actin and F-actin fibers, nerve lysates were fractionated. This analysis revealed that the F-actin to G-actin ratio was increased in mutant nerves when compared to controls at P60. These data suggest that loss of Mtmr2 in KO nerves results in increased F-actin polymerization (Fig. 3 *G* and *G′* and *SI Appendix*, Fig. S3*F*).

Nonmuscular myosin II cross-links with actin filaments thereby forming actomyosin filament bundles. Interestingly, RhoA GTPase and, more directly, ROCK (Rho kinase) and myosin II downstream of RhoA, have been found to be crucial for early stages of PNS myelination (51–53). We thus analyzed the RhoA GTPase pathway in *Mtmr2* KO nerves. To this aim, we first measured active RhoA-GTP levels by performing pull-down assays from mutant and control sciatic nerve lysates at different time points of postnatal development using GST-RBD/Rhotekin recombinant protein, an effector of RhoA GTPase. We observed increased RhoA-GTP levels in *Mtmr2* KO nerves at P2 and P60 (Fig. 4 *A* and *A′* and *SI Appendix*, Fig. S4 *A* and *B*). We then analyzed phosphorylation levels of two known effectors of RhoA, p-MYPT1 (Myosin phosphatase target subunit 1) and p-MLCII (Myosin II light chain-a regulatory subunit of myosin II) (41, 51). Western blot analysis of sciatic nerve lysates revealed an apparent increase of p-MLCII levels in each sciatic nerve pool of *Mtmr2* KO mice analyzed at P2 as compared to controls (Fig. 4*B*). Phosphorylation levels of p-MYPT1 were also increased in *Mtmr2* KO nerves at P60 (Fig. 4 *C* and *C′* and *SI Appendix*, Fig. S4*C*). These data suggest that the RhoA-MLCII pathway is hyperactive in *Mtmr2* KO nerves.

To assess whether enhanced RhoA-mediated signaling occurs specifically in Schwann cells where myelin outfoldings arise, we analyzed nerves of *Mtmr2* cKO^{SC}, a conditional KO with specific inactivation of *Mtmr2* in SCs. Using immunoblot analysis, we found increased p-MYPT1 levels in *Mtmr2* cKO^{SC} nerve lysates (Fig. 4 *D* and *D′* and *SI Appendix*, Fig. S4*D*), thus suggesting that the RhoA pathway overactivation occurs in Schwann cells. Finally, we asked whether increased RhoA activity was specifically associated with CMT4B and myelin outfoldings. To this aim, we tested p-MYPT1 levels in *Pmp22*$^{+/-}$ nerves, a model of the HNPP (hereditary neuropathy with liability to pressure palsies) neuropathy morphologically characterized by tomacula but not myelin outfoldings (54). In *Pmp22*$^{+/-}$ nerves, p-MYPT1 levels were similar to controls (Fig. 4*E* and *SI Appendix*, Fig. S4*E*), thus suggesting that the RhoA pathway elevation is specifically associated with Mtmr2 loss and myelin outfoldings in the nerve.

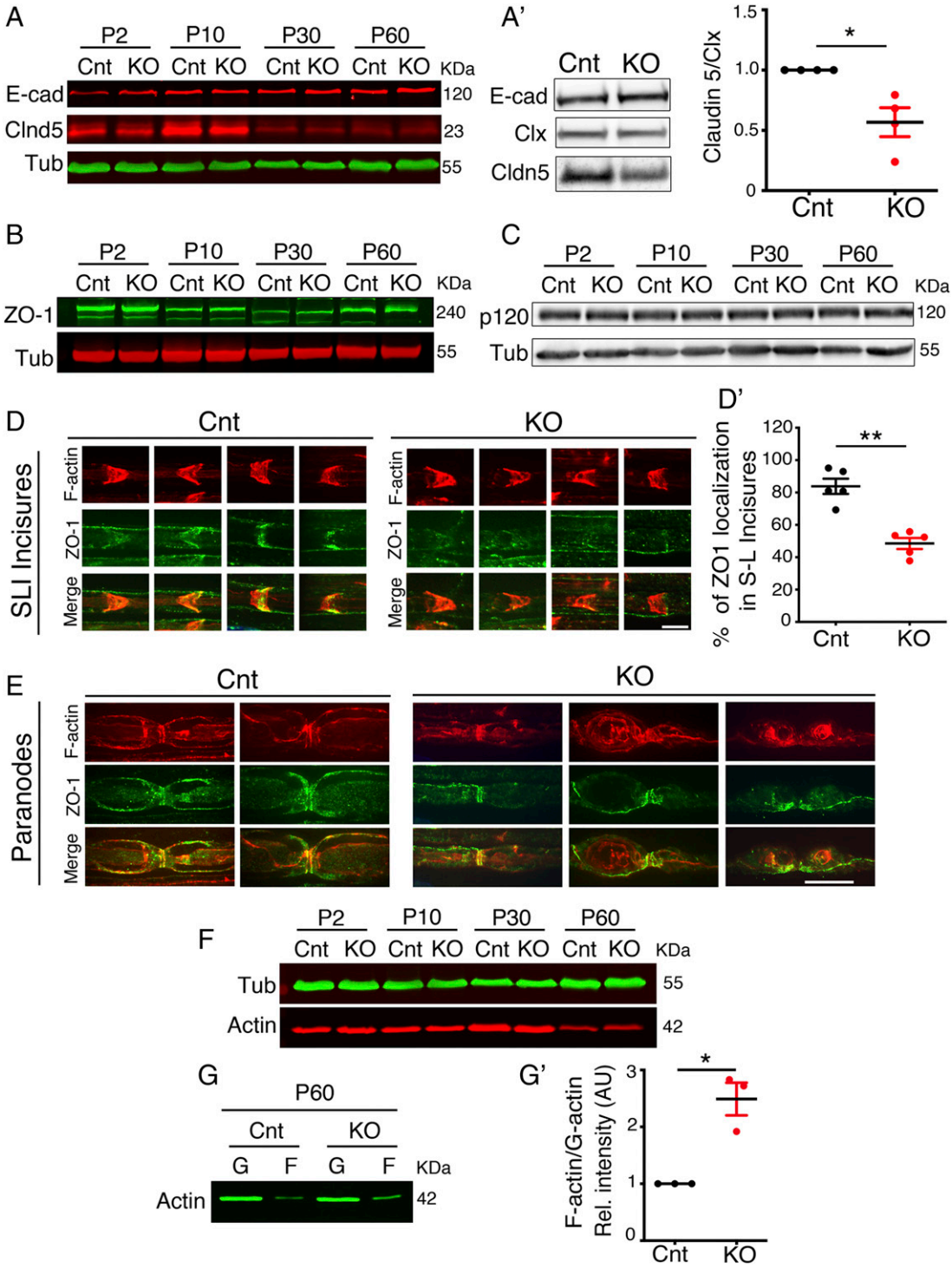

Fig. 3. Altered expression and localization of noncompact myelin markers in *Mtmr2* KO nerves. (*A*–*C*) Western blot analysis of total nerve lysates from *Mtmr2* KO and wild-type control mice (Cnt) at different stages of postnatal development shows that expression levels of E-cadherin, ZO-1, and p120 catenin are similar between mutant and control. Claudin 5 (Cldn5) expression level was decreased in *Mtmr2* KO sciatic nerve lysates at P10 and P30 as quantified in *SI Appendix*, Fig. S2*H*. (*A′*) Western blot analysis performed on membrane fraction lysates from *Mtmr2* KO nerves at P30 confirmed reduced expression levels of claudin 5 in mutant nerves, as quantified in $n = 4$ independent experiments, one-sample *t* test, $^{*}P = 0.0366$, t = 3.606, df = 3. Clx is calnexin used to normalize membrane fraction lysates (*SI Appendix*, Fig. S3 *A*–*D′*). (*D*) Teased fibers analysis of sciatic nerves shows that ZO-1 localization at SLIs was decreased in *Mtmr2* KO nerves at P60. SLIs were stained with phalloidin (F-actin), $n = 5$ animals per genotype in five different experiments; two-tailed Mann–Whitney *U* test, $^{**}P = 0.008$. (*E*) Teased fibers analysis of sciatic nerves shows that ZO-1 localization at paranodal regions is similar in *Mtmr2* KO and control nerves at P60. Paranodes were stained with phalloidin (F-actin). Note that ZO-1 localizes at paranodes also in *Mtmr2* KO fibers carrying myelin outfoldings. (*F*) Western blot analysis of lysates from *Mtmr2* KO nerves and wild-type controls (Cnt) at different stages of postnatal development indicates that expression levels of actin are similar between mutant and control, as quantified in *SI Appendix*, Fig. S3 *E* and *E′*. (*G*) Western blot analysis performed from *Mtmr2* KO nerves at P60 following fractionation of F (polymerized) and G (globular, monomeric) actin shows that the F-actin fraction is increased in mutant nerves, as quantified in G′ with $n = 3$ independent experiments, one-sample *t* test, $^{*}P = 0.0351$, t = 5.196, df = 2 (*SI Appendix*, Fig. S3*F*). (Scale bar, 8 μm in *D* and 11 μm in *E*.)

RhoA Pathway Activation Results in Myelin Outfoldings and Enhanced Actomyosin Contractility in MTMR2/Mtmr2 KO Cells. Next, we asked what the functional consequence of hyperactive RhoA signaling in Schwann cells lacking MTMR2/Mtmr2 might be. To this aim, we first used Schwann cell/DRG neuron coculture explants established from *Mtmr2* KO mice, which reproduce myelin outfoldings. We observed increased MYPT1 phosphorylation in mutant cultures, thus confirming that in vitro as in vivo Mtmr2 loss is associated with RhoA pathway hyperactivation (Fig. 5*A* and *SI Appendix*, Fig. S5 *A* and *A′*). Then, we treated *Mtmr2* KO explants either with Y27632 (at 10 μM), a ROCK inhibitor, or blebbistatin (at 1 μM), a specific inhibitor of nonmuscular myosin II. We observed that both Y27632 (Fig. 5 *C* and *C′*) and blebbistastin (Fig. 5 *E* and *E′*) were able to reduce the fraction of Mbp-positive fibers carrying myelin outfoldings in mutant Schwann cell/DRG neuron coculture explants. Moreover, Y27632 treatment was able to restore MYPT1 phosphorylation to normal levels (Fig. 5*A* and *SI Appendix*, Fig. S5 *A* and *A′*). Of note, in these experimental conditions, Y27632 and blebbistatin did not alter the number of myelin segments or the internodal length (length of myelinated segments) in either control or *Mtmr2* KO cocultures (Fig. 5 *B*, *B′*, and *D*–*D″* and *SI Appendix*, Fig. S6 *A*–*B′*). Of note, a reduction in the length of myelinated segments could be observed at higher concentrations of blebbistatin in similar experimental conditions, as Myosin II is a promoter of Schwann cell elongation during early stages of PNS myelination (53).

To further assess the functional consequences of enhanced RhoA activation in MTMR2/Mtmr2 KO cells, we exploited primary fibroblasts from CMT4B1 patients, in which PtdIns(3,5)P_2 levels are increased (Fig. 1*B*). First, we assessed whether the RhoA pathway is also activated in these cells that lack MTMR2 similar to nerves from *Mtmr2* KO mice (Fig. 4) and Schwann cell/DRG neuron cocultures (Fig. 5*A*). As expected, we found p-MYPT1 levels to be increased in CMT4B1 patient fibroblasts (*SI Appendix*, Figs. S7*B* and S5*B*). To evaluate the functional impact of enhanced RhoA signaling, we monitored these cells during adhesion, a process that requires extensive morphological changes and actomyosin cortical cytoskeleton rearrangements. Interestingly, we noted that an increased number of CMT4B1 cells had a round morphology compared to controls (*SI Appendix*, Fig. S7 *A*–*A″*). These findings suggest that in CMT4B1 fibroblasts elevation of PtdIns(3,5)P_2 is associated with enhanced

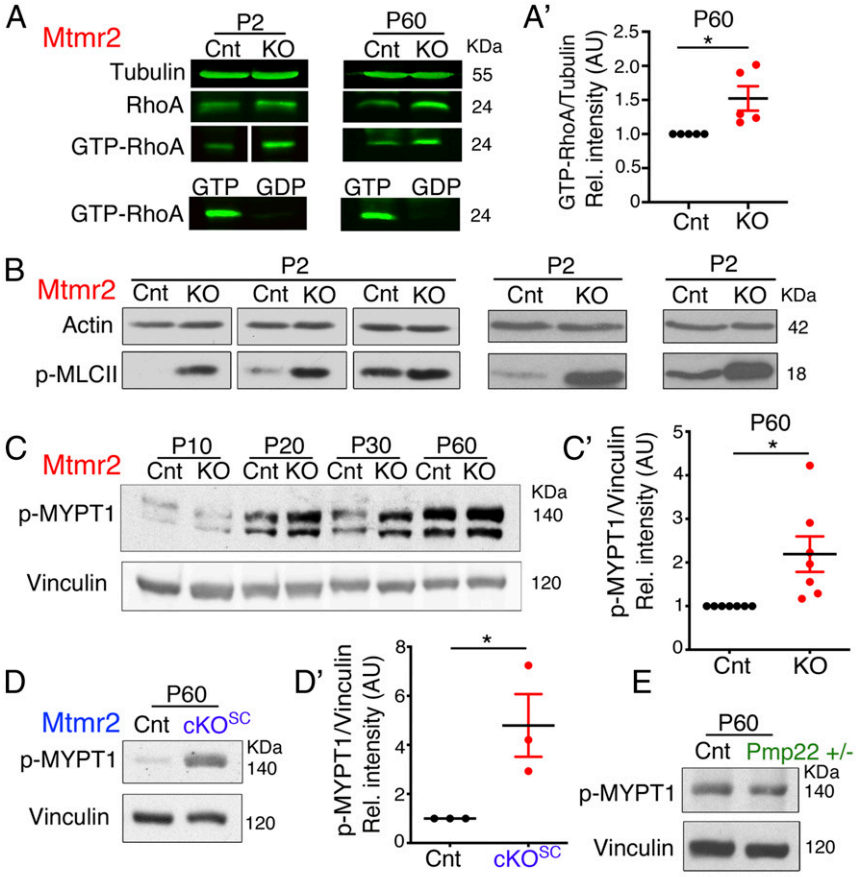

Fig. 4. Increased RhoA-myosin II pathway in *Mtmr2* KO nerves. (*A*) Pull-down assay from *Mtmr2* KO and control sciatic nerves at P2 and P60 using GST-RBD/Rhotekin as a bait to detect active GTP-bound RhoA. GTPγS and GDP were used as control to check the GST-RBD/Rhotekin recombinant protein. Representative data from two independent experiments at P2 and five at P60 (*SI Appendix*, Fig. S4 *A* and *B*). (*A′*) Quantification of the active RhoA-GTP GST-bound fraction at P60 in control and mutant nerves, $n = 5$ independent experiments, one-sample *t* test, $^*P = 0.0438$, t = 2.907, df = 4. (*B*) Western blot analysis shows an apparent increase of p-MLCII levels in each sciatic nerve pool of *Mtmr2* KO mice analyzed as compared to controls. Three independent experiments. (*C*) Western blot analysis indicates that phosphorylation of the MYPT1 phosphatase downstream of RhoA is increased in *Mtmr2* KO sciatic nerve lysates at P20, P30, and P60, and quantified in *C′*, $n = 7$ animals per genotype in four independent experiments, one-sample *t* test, $^*P = 0.0264$, t = 2.926, df = 6 (*SI Appendix*, Fig. S4*C*). (*D*) Western blot analysis indicates that phosphorylation of the MYPT1 phosphatase is increased in *Mtmr2*$^{Floxed/Floxed}$; *P0-Cre* (the conditional KO of *Mtmr2* in Schwann cells, cKO^{SC}) sciatic nerve lysates at P60, and quantified in D′, $n = 3$ animals per genotype in two independent experiments, one-sample *t* test, one tail, $^*P = 0.0486$, t = 2.967, df = 2 (*SI Appendix*, Fig. S4*D*). (*E*) Phosphorylation levels of MYPT1 are similar between control and *Pmp22*$^{+/-}$ mutant nerves, $n = 3$ animals per genotype in two independent experiments, one-sample *t* test, $P = 0.2478$, t = 1.615, df = 2 (*SI Appendix*, Fig. S4*E*).

cortical actomyosin remodeling, a process that depends on RhoA GTPase activity.

Altogether, these data indicate that loss of MTMR2/Mtmr2 leads to enhanced RhoA GTPase signaling in vivo and ex vivo and that dysregulation of this pathway may contribute to the CMT4B1 phenotype.

PtdIns(3,5)P_2 Elevation Triggers RhoA Pathway Activation in *Mtmr2* KO Cells. In MTMR2/Mtmr2 KO cells and nerves elevated PtdIns(3,5)P_2 levels are associated with both increased mTORC1 and RhoA GTPase signaling. While mTORC1 is a known effector of PtdIns(3,5)P_2 (25, 26), the association between this phosphoinositide and RhoA has not been previously reported. Thus, we sought to assess whether PtdIns(3,5)P_2 is upstream of RhoA and the actomyosin cytoskeleton. To this aim, we monitored the RhoA GTPase pathway activation following down-regulation or up-regulation of PtdIns(3,5)P_2 levels.

To down-regulate PtdIns(3,5)P_2, we took advantage of primary fibroblasts from *Mtmr2*$^{-/-}$ and from *Mtmr2*$^{-/-}$; *Fig4*$^{+/-}$ double mutant mice, in which PtdIns(3,5)P_2 should be rebalanced. Mtmr2 facilitates PtdIns(3,5)P_2 turnover, whereas Fig4 is a PIKfyve activator. As a result, Fig4 and Mtmr2 compensate each other's loss, resulting in rebalanced PtdIns(3,5)P_2 levels as previously reported (18, 25). Similar to CMT4B1 patient fibroblasts, we observed that, during adhesion, *Mtmr2* KO cells displayed a round morphology with increased central stress fibers distribution, whereas *Mtmr2*$^{-/-}$; *Fig4*$^{+/-}$ double mutant fibroblasts were similar to control (*SI Appendix*, Fig. S7 *D*, *D′*, and *E*). As seen in CMT4B1 patient fibroblasts, this phenotype correlated with increased RhoA signaling. Increased p-MLC levels were detected in *Mtmr2* KO cells, whereas p-MLC was similar between wild-type and *Mtmr2*$^{-/-}$; *Fig4*$^{+/-}$ double mutant cells (*SI Appendix*, Figs. S7 *C* and *C′* and S5 *C* and *D*). Finally, following the hypothesis that *Mtmr2* KO mutant fibroblasts with enhanced actomyosin contractility and a rounder shape should migrate less, we tested the ability of *Mtmr2* KO fibroblasts to fill the wound in wound-healing assays. Consistent with our hypothesis, *Mtmr2* KO fibroblasts displayed reduced motility compared to controls and this impaired migratory phenotype was almost completely restored in *Mtmr2*$^{-/-}$; *Fig4*$^{+/-}$ cells (*SI Appendix*, Fig. S7*F*). These data suggest that in fibroblasts lacking MTMR2/Mtmr2 enhanced PtdIns(3,5)P_2 levels result in RhoA hyperactivation and increased actomyosin contractility. Consistent with this, down-regulation of PtdIns(3,5)P_2 levels reduced RhoA activation and actomyosin contractility.

To further assess whether PtdIns(3,5)P_2 and RhoA act in the same pathway in myelinating nerves, we treated *Mtmr2* KO Schwann cell/DRG neuron coculture explants with myelin outfoldings using apilimod (the PIKfyve inhibitor) plus blebbistatin (the myosin II inhibitor) or using either apilimod or blebbistatin. We found that apilimod and blebbistatin together displayed the same efficiency in reducing the percentage of Mbp-positive fibers carrying myelin outfoldings on the total number of Mbp-positive fibers as compared to single treatments (Fig. 6 *A*–*C*). These data suggest that PtdIns(3,5)P_2 and RhoA act in the same pathway to regulate myelin growth.

Finally, we assessed whether addition of exogenous short chain membrane-permeant PtdIns(3,5)P_2 can trigger RhoA pathway hyperactivation. We administered PtdIns(3,5)P_2 to wild-type and *Mtmr2* KO Schwann cell/DRG neuron coculture explants. Immunoblot analysis showed that exogenous application of PtdIns(3,5)P_2 but not of PtdIns3*P* boosted MYPT1 phosphorylation in *Mtmr2* KO cultures (Fig. 6 *D* and *D′* and *SI Appendix*, Fig. S5*E*).

Taken together, these findings indicate that loss of MTMR2/Mtmr2 results in increased PtdIns(3,5)P_2 levels, which triggers RhoA pathway hyperactivation. Increased RhoA modifies actomyosin cytoskeletal dynamics ultimately resulting in myelin outfoldings.

Down-Regulation of PIKfyve Activity as a Strategy to Ameliorate CMT4B1. Our data suggest that elevation of PtdIns(3,5)P_2 dysregulates mTORC1-dependent myelin synthesis and actomyosin function, ultimately leading to defective myelin longitudinal growth in CMT4B1. Consistent with this, rebalancing PtdIns(3,5)P_2 levels could represent an effective therapeutic strategy for CMT4B1, as already observed using several approaches aimed at decreasing PIKfyve activity and PtdIns(3,5)P_2 levels in *Mtmr2* KO models (18).

Indeed, we observed that apilimod was able to reduce myelin outfoldings in Schwann cell/DRG neuron coculture explants from *Mtmr2* KO mice. Since apilimod displays high affinity for PIKfyve and crosses the blood–brain barrier, we tested whether this drug could represent an effective therapeutic strategy for CMT4B1 in vivo. To this aim, apilimod was administered to *Mtmr2* KO mice by gavage starting at P60 during disease course once a day (QD) at 60 mg/kg, which is below the highest concentration tolerated in mice in a chronic treatment setting. Neurophysiological and morphological analyses of sciatic nerves were performed at 6 mo. Neurophysiological analyses showed that apilimod treatment was able to ameliorate defects in nerve conduction velocity (NCV) in *Mtmr2* KO apilimod-treated mice compared to vehicle-treated *Mtmr2* KO, which display reduced NCV (Fig. 7*A*). However, apilimod treatment initiated at P60 was unable to reduce the percentage of myelin outfoldings in *Mtmr2* KO nerves (Fig. 7 *B* and *D*). Morphometric analyses showed that apilimod treatment did not affect myelin thickness indicated by an unaltered g-ratio (Fig. 7 *C* and *D*).

These data suggest that, using this treatment protocol and timing, apilimod is effective in ameliorating nerve conduction velocity without reducing the number of myelin outfoldings.

Discussion

CMT4B1 is an autosomal recessive demyelinating neuropathy with childhood onset, characterized by the presence of myelin outfoldings in the nerve, a pathological aberrant form of myelination (4). This morphology may be the consequence of an excessive longitudinal growth of the myelinated internode during postnatal nerve development. Myelin outfoldings are thought to alter nerve physiology, leading to myelin and fiber degeneration, which correlate with the clinical outcome (5). Interestingly, this aberrant form of myelin consists of redundant folds of Schwann cell membrane and axon running in parallel to the myelinated internode, which preferentially arise at noncompact myelin regions (32–36). Thus, MTMR2 can be considered as a negative regulator of membrane growth and myelin outfoldings as a model of excessive longitudinal myelin growth. Here we propose a mechanism by which MTMR2, by regulating PtdIns(3,5)P_2 levels, coordinates mTORC1-dependent myelin synthesis and RhoA/myosin II-dependent cytoskeletal dynamics necessary to expand the membrane and promote longitudinal myelin growth.

Our results are consistent with and extend previous data from nonmyelin-forming cells suggesting that PtdIns3*P* and PtdIns(3,5)P_2 can locally facilitate nutrient signaling by mTORC1 at late endosomes and lysosomes (25, 26) and from KO Schwann cells lacking the MTMR13/MTMR2-associated small GTPase Rab35 that display mTORC1 hyperactivation as a consequence of defective PtdIns(3,5)P_2 hydrolysis (19). Here, we extend these findings by demonstrating that mTORC1 is overactivated in *Mtmr2* KO cells, in which PtdIns(3,5)P_2 levels are elevated (18). Consistently, we found that application of the known mTORC1 inhibitor rapamycin ameliorates myelin outfoldings in *Mtmr2* KO Schwann cell/DRG neuron cocultures.

Importantly, we now demonstrate that aberrant myelin in the absence of MTMR2 is not merely a consequence of altered mTORC1 activity but also relates to overactive RhoA signaling caused by elevated PtdIns(3,5)P_2 levels. These results are in line with and significantly extend the established function of RhoA

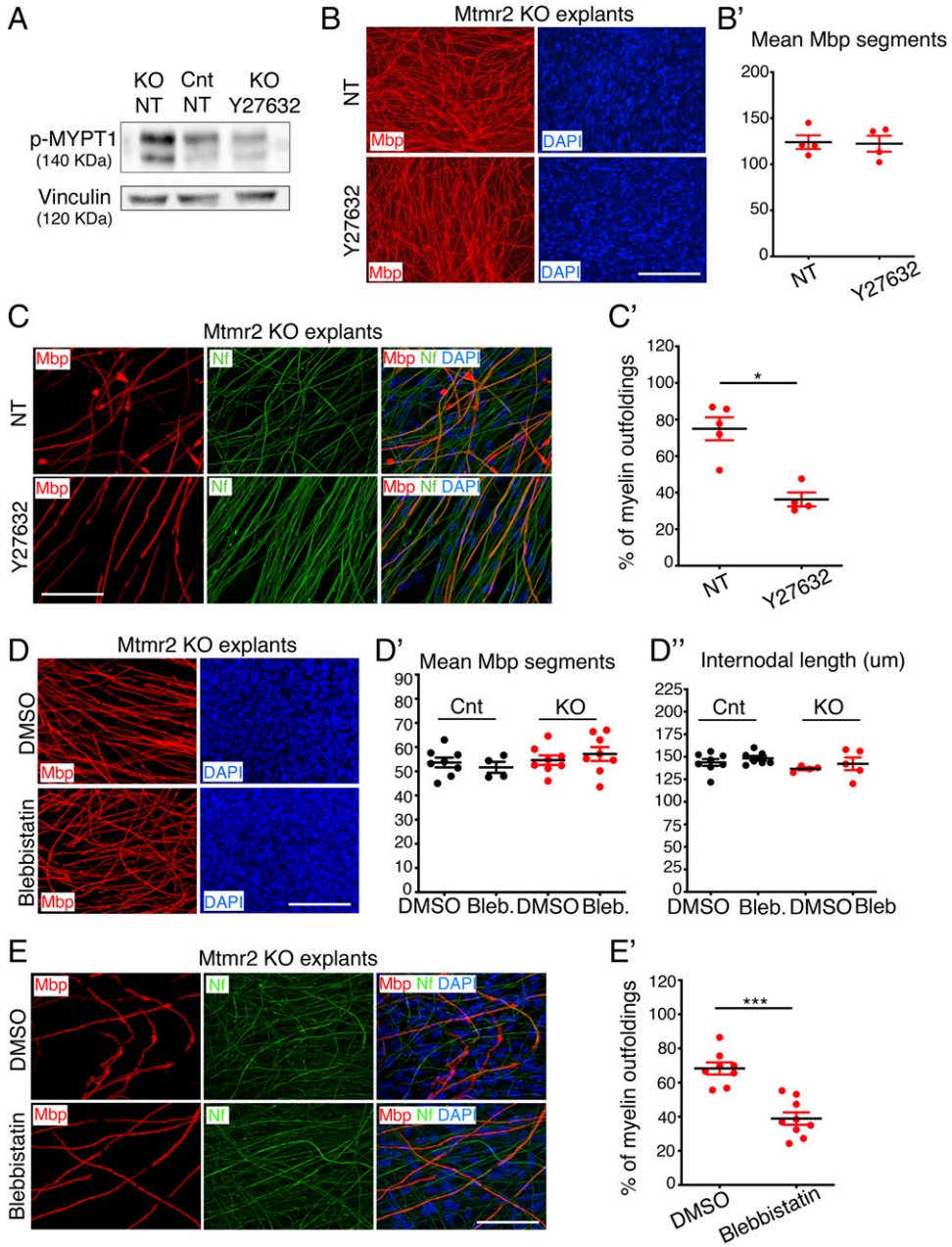

Fig. 5. Inhibition of the RhoA-myosin II pathway rescues myelin outfoldings. (*A*) Western blot analysis shows that phosphorylation of MYPT1 is increased in *Mtmr2* KO Schwann cell/DRG neuron coculture lysates as compared to controls (NT, not treated) and that treatment using the ROCK inhibitor Y27632 restores phosphorylation to normal levels. Representative of two independent experiments performed using a total of three pools of DRG/coverslips per condition per genotype (*SI Appendix*, Fig. S5 *A* and *A'*). (*B*) Y27632 treatment does not interfere with myelination in *Mtmr2* KO Schwann cell/DRG neuron coculture explants as assessed by measuring the number of Mbp-positive fibers after 14 d of ascorbic acid treatment in differentiating conditions. Mbp-positive segments quantified in B′: $n = 4$ DRG/coverslips NT and $n = 4$ DRG/coverslips Y27632-treated, two-tailed Mann–Whitney *U* test, $P = 0.886$. Representative of two independent experiments. (*C*) Y27632 treatment rescues myelin outfoldings in *Mtmr2* KO Schwann cell/DRG neuron coculture explants as assessed by confocal microscopy analysis of Mbp-positive fibers carrying myelin outfoldings on the total number of Mbp-positive fibers and quantified in C′. $n = 5$ DRG/coverslips NT, at least 200 total fibers analyzed, and $n = 4$ DRG/coverslips Y27632-treated, at least 200 total fibers analyzed, two-tailed Mann–Whitney *U* test, $*P = 0.016$. Representative of two independent experiments. (*D*) Treatment with 1 μM blebbistatin, a myosin II inhibitor, does not interfere with myelination in both control and in *Mtmr2* KO Schwann cell/DRG neuron coculture explants after 14 d of ascorbic acid treatment in differentiating conditions. *D′*: quantification of the number of Mbp-positive segments in wild-type cocultures, $n = 8$ DRG/coverslips DMSO-treated and $n = 4$ DRG/coverslips blebbistatin-treated and in *Mtmr2* KO explants, $n = 8$ DRG/coverslips DMSO-treated and $n = 8$ DRG/coverslips blebbistatin-treated, $P = 0.5483$, nonparametric one-way ANOVA, followed by Dunn's post hoc test, representative of two independent experiments. *D′′*: quantification of the length of Mbp-positive segments (internodal length in micrometers) in wild-type cocultures, $n = 8$ DRG/coverslips DMSO-treated and $n = 7$ DRG/coverslips blebbistatin-treated and in *Mtmr2* KO explants, $n = 4$ DRG/coverslips DMSO-treated and $n = 5$ DRG/coverslips blebbistatin-treated, nonparametric one-way ANOVA, followed by Dunn's post hoc test, $P = 0.1203$. (*E*) Blebbistatin treatment rescues myelin outfoldings in *Mtmr2* KO Schwann cell/DRG neuron coculture explants as assessed by confocal microscopy analysis of Mbp-positive fibers carrying myelin outfoldings on the total number of Mbp-positive fibers and quantified in *E′*. $n = 8$ DRG/coverslips DMSO-treated, at least 300 total fibers analyzed and $n = 9$ DRG/coverslips blebbistatin-treated, at least 300 total fibers analyzed, two-tailed Mann–Whitney *U* test, $***P < 0.0001$. Representative of three independent experiments. Mbp, Myelin basic protein; Nf, neurofilament. (Scale bar, 155 μm in *B*; 58 μm in *C*; 167 μm in *D*, and 56 μm in *E*.)

and nonmuscular myosin II in Schwann cell membrane longitudinal extension that precedes Rac1/Cdc42-mediated radial lamellipodia protrusion formation during radial sorting in PNS development (52, 53, 55). We propose that MTMR2 loss and the resulting increase of PtdIns(3,5)P_2 overactivate RhoA-myosin II and enhance actomyosin contractility at noncompact myelin "apical-like" regions. Interestingly, two forms of CMT neuropathies have also been associated with a gain of function of RhoA GTPase activity. Mutations in *ARHGEF10*, a RhoA regulator, result in RhoA activation and CMT neuropathy (56). Loss of function of *INF2*, another RhoA regulator, results in RhoA activation and CMT neuropathy. Interestingly, myelin outfoldings have been observed in a CMT patient biopsy with *INF2* mutation (57). Other models further support the involvement of actin cytoskeletal remodeling in the formation of myelin outfoldings. Loss of function of N-WASP, Cdc42, and of atypical PKC have all been associated with myelin outfoldings (44, 47, 48). Moreover, loss of Cadm4, which is localized in the apical-like regions of Schwann cells, results in myelin outfoldings (45). Cadm4 interacts with protein 4.1B and is connected with the actin cytoskeleton underneath the Schwann cell adaxonal membrane. Finally, in the CNS, spatially unrestricted branched F-actin disassembly results in aberrant myelin membrane growth and myelin outfolding formation (49, 50). Collectively, our data reported here suggest that lipid-mediated enhancement of actomyosin contractility together with elevated mTORC1 signaling in the absence of MTMR2 underlies the formation of myelin outfoldings in the PNS.

Whether these signaling pathways act in parallel or whether mTORC1 directly or indirectly controls RhoA remains to be clarified. In the first case, phosphoinositide-dependent mTORC1 signaling and cytoskeleton remodeling might be concomitantly necessary in "a double hit process" for myelin membrane expansion at sites of myelin growth. This cooperation is supported by other pathological models. Genetic down-regulation of the PTEN phosphatase in Schwann cells leads to altered PtdIns(3,4,5)P_3 and PtdIns(4,5)P_2 levels, two known regulators of mTORC1 and cytoskeleton remodeling. *Pten* KO mutant nerves display increased myelin thickness and aberrant myelin (30). Similarly, constitutive AKT activation in Schwann cells results in increased myelin

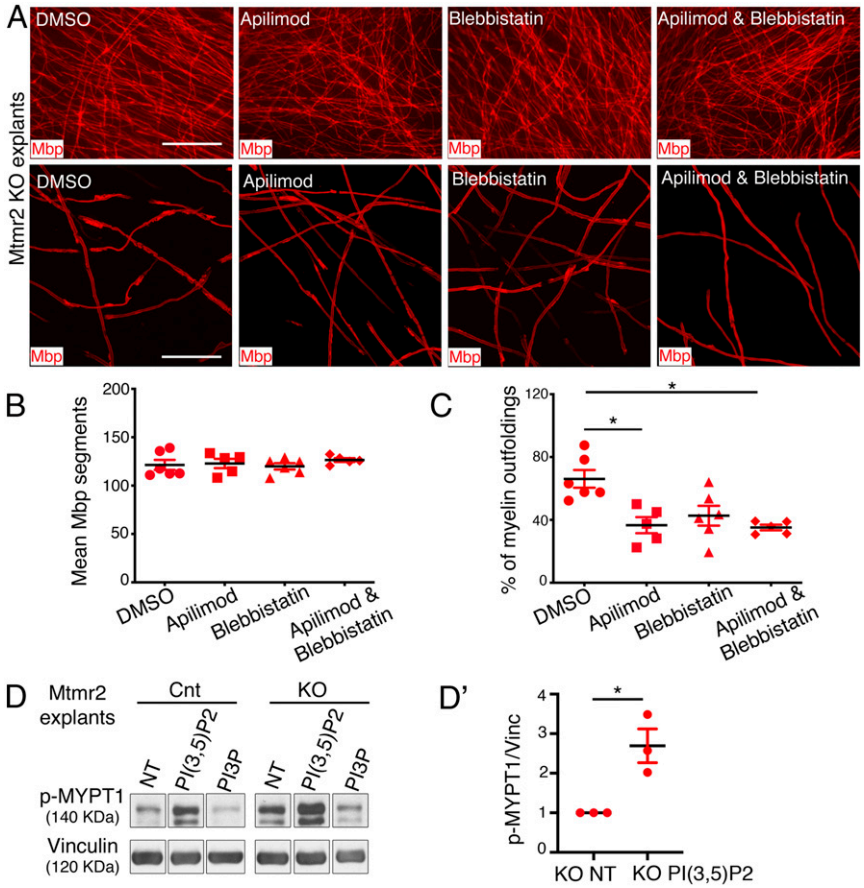

Fig. 6. Enhanced PtdIns(3,5)P_2 triggers RhoA-myosin II activation. (*A*) Representative fluorescence microscope images (*Upper*) and confocal microscope images (*Lower*) of *Mtmr2* KO Schwann cell/DRG neuron coculture explants treated for 14 d in differentiating conditions with DMSO, apilimod, blebbistatin, and apilimod plus blebbistatin and stained for Mbp. (*B*) Quantification of the Mbp-positive segments in the *Mtmr2* KO Schwann cell/DRG neuron coculture explants treated as indicated for 14 d in differentiating conditions. DMSO-treated, $n = 6$ DRG/coverslips; apilimod-treated, $n = 5$ DRG/coverslips; blebbistatin-treated, $n = 6$ DRG/coverslips, and apilimod plus blebbistatin-treated, $n = 5$ DRG/coverslips, nonparametric one-way ANOVA followed by Dunn's post hoc test, $P = 0.6520$, representative of two independent experiments. (*C*) Quantification of the number of Mbp-positive fibers carrying myelin outfoldings on the total number of Mbp-positive fibers analyzed. DMSO-treated, $n = 6$ DRG/coverslips, 210 fibers; apilimod-treated, $n = 5$ DRG/coverslips, 204 fibers; blebbistatin-treated, $n = 6$ DRG/coverslips, 218 fibers, and apilimod plus blebbistatin-treated, $n = 5$ DRG/coverslips, 206 fibers analyzed, nonparametric one-way ANOVA followed by Dunn's post hoc test, $*P = 0.0107$, representative of two independent experiments. DMSO and apilimod, $*P = 0.04$; DMSO and apilimod plus blebbistatin, $*P = 0.018$. (*D*) Western blot analysis of wild-type control and *Mtmr2* KO Schwann cell/DRG neuron coculture explant lysates following treatment with C4-PtdIns(3,5)P_2 or C4-PtdIns3*P* phosphoinositides. Phosphorylation levels of MYPT1 are increased in *Mtmr2* KO as compared to control and PtdIns(3,5)P_2 treatment further increases phosphorylation, as quantified in *D'*, $n = 3$ independent experiments, one-sample *t* test, one tail, $*P = 0.029$ (*SI Appendix*, Fig. S5*E*). Mbp, myelin basic protein. (Scale bar in *A*, *Upper*, 124 μm [fluorescence microscope images] and *Lower*, 46 μm [confocal microscope images].)

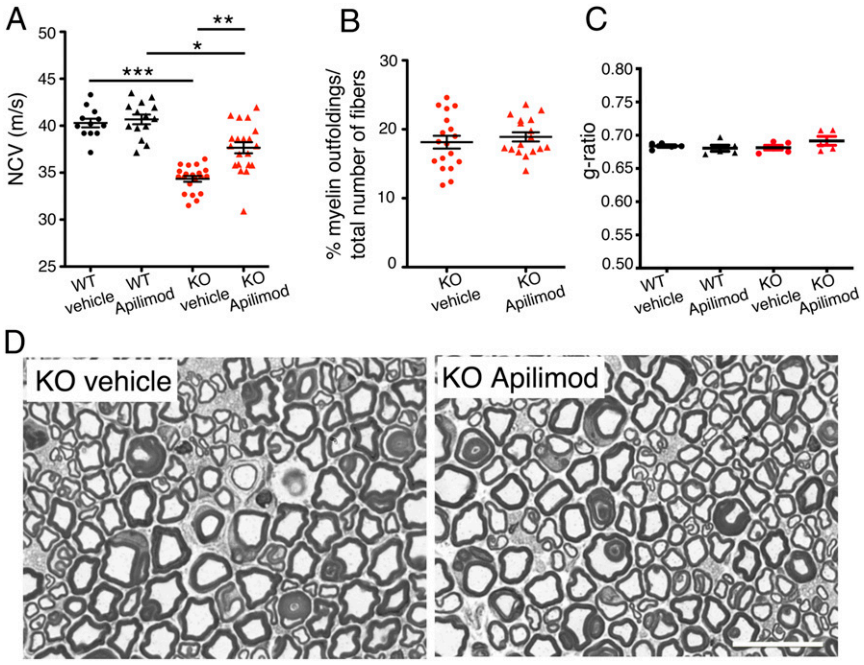

Fig. 7. Apilimod rescues nerve conduction velocity in *Mtmr2* KO mice. (*A*) Nerve conduction velocity values (m/s) measured in wild-type (WT) and *Mtmr2* KO sciatic nerves after vehicle or apilimod treatment by gavage daily (QD) starting at P60 for 4 mo, wild-type vehicle-treated, $n = 12$; wild-type apilimod-treated, $n = 14$; *Mtmr2* KO vehicle-treated, $n = 20$; *Mtmr2* KO apilimod-treated, $n = 20$, nonparametric one-way ANOVA followed by Dunn's post hoc test, $***P < 0.0001$. WT vehicle and WT apilimod, $P > 0.9999$; WT vehicle and KO vehicle, $***P < 0.0001$; WT apilimod and KO apilimod, $*P = 0.0324$; KO vehicle and KO apilimod, $**P = 0.0029$. (*B*) Semithin section analysis of sciatic nerves from *Mtmr2* KO vehicle-treated and apilimod-treated at 6 mo shows a similar number of fibers carrying myelin outfoldings, two-tailed Mann–Whitney *U* test, $P = 0.5198$. (*C*) The g-ratio, the ratio between axon diameter and fiber diameter-axon plus myelin, is similar between wild-type and *Mtmr2* KO sciatic nerve vehicle or apilimod-treated, ultrastructural analysis, nonparametric one-way ANOVA followed by Dunn's post hoc test, $P = 0.5098$, $n = 5$ animals and at least 300 fibers analyzed per group. (*D*) Representative images of semithin section analysis of sciatic nerves from *Mtmr2* KO vehicle-treated and apilimod-treated mice. (Scale bar in *D*, 18 μm.)

thickness, aberrant myelin, and in enhanced Rac1 GTPase activity, which is a known regulator of actin cytoskeleton remodeling (31). Consistent with these findings, constitutive activation of mTORC1 following TSC1/2 depletion in Schwann cells results in aberrant myelination (27–29).

How PtdIns(3,5)P_2 may promote RhoA activity remains to be assessed. We can speculate that enhanced PtdIns(3,5)P_2 may alter membrane recruitment of a RhoA regulator or that, alternatively, PtdIns(3,5)P_2 may directly interact with RhoA. This scenario could be supported by the presence of a basic region (QARRG) at the C terminus of RhoA, which resembles the consensus sequence of WIPI proteins, conserved autophagy regulatory proteins known to bind both PtdIns3*P* and PtdIns(3,5)P_2 (58). Of note, even if the putative binding sequence is not fully conserved, the two basic residues of this sequence are also present in RhoC, which was identified as a potential PtdIns(3,5)P_2 binding protein (59).

In a second scenario, mTORC1 may control or intersect with RhoA signaling. Interestingly, mTORC1 and mTORC2 have been shown to regulate motility of colorectal cancer cells via RhoA and Rac1 signaling (60). Other studies suggested that both mTORC1 and mTORC2 are involved in regulating F-actin reorganization and formation of lamellipodia in a panel of cancer cells (61, 62). This regulation could be due in part to enhanced RhoA protein expression and/or activity mediated by mTORC1-S6K1-4EBP1 signaling (63). Finally, during neutrophil chemotaxis, mTORC2 has been shown to specifically regulate Myosin II through a cAMP/RhoA signaling axis, independently of actin reorganization (64).

A common denominator of both of these phenotypes, hyperactive mTORC1 and increased RhoA signaling resulting in aberrant myelin, appears to be the regulation of PtdIns(3,5)P_2 levels by MTMR2. Hence, CMT4B1 would be expected to be ameliorated by strategies aimed at rebalancing PtdIns(3,5)P_2 levels. An ideal target is PIKfyve, the kinase that produces PtdIns(3,5)P_2 and counteracts MTMR2 phosphatase activity. Lipid kinase inhibition is a therapeutic strategy in cancer and, more recently, has also been found to be effective in genetic disorders due to PI3K overactivation (65). However, contrary to PI3K inhibition, few small molecule compounds targeting PIKfyve have been developed so far. Apilimod is a recently identified PIKfyve inhibitor, which displays high affinity for PIKfyve (20, 66). Our preclinical studies using apilimod in the *Mtmr2* KO model indeed suggest that this drug is effective in ameliorating nerve conduction velocity, i.e., a functional measure of the nerve. However, contrary to our data from *Mtmr2* KO cocultures, using this treatment protocol and timing apilimod was ineffective in reducing myelin outfoldings in vivo in *Mtmr2* KO mice. Hence, alternative therapeutic strategies may be needed, for example combined pharmacological inhibition of mTORC1 and/or RhoA/myosin II, the PtdIns(3,5)P_2 downstream targets. However, at this point it also cannot be ruled out that the slowing of nerve conduction does not only represent a consequence of demyelination and the formation of myelin outfoldings at least during earlier stages of disease. Additional studies will be required to address these and other issues.

Materials and Methods

Mice. The generation and characterization of the full *Mtmr2*$^{-/-}$ KO mouse; of the *Mtmr2*$^{Floxed/Floxed}$; *P0-Cre* conditional KO mouse (cKO) in Schwann cells, and of the *Pmp22*$^{+/-}$ mutant have been previously reported (35, 36, 54). The *Mtmr2* KO mouse reported in this study has been backcrossed in 129SV/Pas for $n = 9$ generations. The characterization of the *Fig4*$^{-/+}$ allele (*Plt*, pale tremor mouse) has been previously reported along with the generation of *Mtmr2*$^{-/-}$; *Fig4*$^{+/-}$ double mutant mice used in this study to establish primary fibroblasts (18).

Preclinical trials were performed by treating *Mtmr2* KO and wild-type mice using apilimod dimesylate (AI Therapeutics).

All animal experiments were conducted according to the guidelines of the Italian national regulations and covered by experimental protocols reviewed by local institutional animal care and use committees.

Schwann Cell/DRG Neuron Cocultures. Myelin-forming Schwann cell/DRG neuron coculture organotypic explants have been established from *Mtmr2* KO at E13.5 as already reported (22). DRGs are isolated from spinal cords and one DRG is plated onto the center of each collagen-coated 12-mm German glass coverslip as reported (22).

To quantify the amount of myelinated segments, using a fluorescence microscope at least 5 to 10 fields/coverslip were randomly acquired and Mbp-positive myelinated fibers were counted per field. Means of each DRG/coverslip have been used as different "*n*" for statistical analysis. To quantify the number of Schwann cell nuclei, using a fluorescence microscope at least 5 fields/coverslip were randomly acquired and DAPI-positive Schwann cell nuclei were counted per field. Means of each DRG/coverslip have been used as different *n* for statistical analysis.

To quantify myelinated fibers carrying myelin outfoldings, at least 200 Mbp-positive myelinated fibers were evaluated, from *n* different DRG explants/coverslips using a TCS SP5 laser-scanning confocal microscope (Leica). The percentage of Mbp-positive fibers showing altered myelin among the total number of Mbp-positive fibers was indicated. Detailed methods are provided in *SI Appendix, Materials and Methods*.

Primary Fibroblast Cultures. Mouse primary fibroblasts were established and cultured as reported using Dulbecco's modified Eagle medium (DMEM) and 10% fetal bovine serum supplemented with 2 mM sodium pyruvate (18). Human primary fibroblasts were established from skin biopsy samples and cultured at 5% O_2 and 5% CO_2 using DMEM and 10% fetal bovine serum supplemented with 2 mM sodium pyruvate. Detailed methods are provided in *SI Appendix, Materials and Methods*.

Patients gave informed consent to clinical and functional studies according to respective national regulations and in agreement with the Declaration of Helsinki (64th WMA General Assembly, Fortaleza, Brazil, October 2013). The clinical study was approved by the Ethics Committee of the Fondazione IRCCS Istituto Neurologico Carlo Besta and IRCCS Ospedale San Raffaele, Milan, Italy. Patient material was collected and anonymized.

Phosphoinositide Analysis and Cell Treatment. To quantify phosphoinositides, human fibroblasts were plated at 1.10^6 cells in 10-cm^2 dishes and their culture media were changed every day until a confluence of 80 to 90% was achieved. Cells were then labeled for 16 h in phosphate-free DMEM containing 200 μCi/mL [^{32}Pi]-orthophosphate. Lipids were then extracted, separated by thin layer chromatography, deacylated, and analyzed by high-performance liquid chromatography using a strong anion exchanger column (Partisphere 5 SAX; Whatman) coupled to a continuous flow in-line scintillation detector (Beckman Instrument) as previously described (67).

For treatment with exogenous short-chain phosphoinositides, C4-PtdIns3*P* and C4-PtdIns(3,5)P_2 (Echelon Biosciences Inc.) were resuspended in phosphate-buffered saline (PBS) and used at 15 μM for 60 min on serum-starved cells.

Western Blot Analysis, Pull-Down Analysis, and Nerve Fractionation. To prepare protein lysates from sciatic nerves, pools of at least 14 nerves at P2; 6 nerves at P10; 4 nerves at P20 and at P30, and 2 nerves at P60 were used. Protein lysates from DRG cocultures were prepared from pools of at least 10 DRG/coverslips per condition/genotype. RBD-Rhotekin cDNA was cloned into pGEX-4T2 expression vector and expressed together with GST in *Escherichia coli* BL21 (DE3) cells. Detailed methods are provided in *SI Appendix, Materials and Methods*.

Membrane and cytosolic fractions from sciatic nerves were obtained using the membrane protein extraction kit (Abcam, ab65400), following manufacturer's instructions. Pools of eight nerves from four animals per genotype were used at P30.

F/G-actin fractionation was performed using the F/G-actin fractionation assay (Cytoskeleton, BK037), following manufacturer's instructions. Pools of eight nerves from four animals per genotype were used at P60.

Immunofluorescence on Teased Fibers. For teased fiber preparation, sciatic nerves were removed, fixed on ice in freshly prepared buffered 4% paraformaldehyde for 30 min, and washed three times in PBS. Then the nerves were placed in a Petri dish with cold PBS, the perineurium was removed, and segments were subdivided with fine needles into fine fascicles of nerve fibers. Detailed methods are provided in *SI Appendix, Materials and Methods*.

Morphological Analysis. Semithin analysis of sciatic nerves and ultrastructural analysis of sciatic nerves were performed as described previously (36). Detailed methods are provided in *SI Appendix, Materials and Methods*.

Statistical Analysis. Power analyses were performed using GPower software, v. 3.1, based on a two independent sample Mann–Whitney *U* test with a significance level α set equal to 5%.

For each analysis, we evaluated whether the assumption required for correct application of standard parametric tests were met. Thus, a two-tailed nonparametric Mann–Whitney *U* test was performed to compare two independent groups. A one-sample *t* test was instead performed to assess whether the median of ratios was greater than 1. The exact *P* value was calculated.

In presence of more than two groups, a Kruskal–Wallis test, the nonparametric one-way ANOVA counterpart, was applied followed by Dunn's post hoc correction.

Data Availability. All study data are included in the article and/or *SI Appendix*.

ACKNOWLEDGMENTS. Apilimod dimesylate was provided by AI Therapeutics, Guilford, CT. We thank Drs. Carmen Melendez-Vasquez, Julien Viaud, and Karim Hnia for useful discussion. We are also grateful to Dr. Stefano Previtali for critical reading of the manuscript. We thank Rossana Tonlorenzi and Stefania Banfi for the excellent technical assistance. Research in this paper was supported by the following: to A.B. by Joint Transnational Call (JTC) 2015 CMT-NRG, E-Rare JTC 2017 TREAT-MTMs, Muscular Dystrophy Association (MDA574294), Telethon-Italy #GGP15012A, and Association Française contre les Myopathies (AFM)-Telethon France #21528, and the Italian Ministry of Health #RF-2016-02361246; to B.P. by E-Rare JTC 2017 TREAT-MTMs and AFM-Telethon France #21528; to V.H. by E-Rare JTC 2017 TREAT-MTMs (Deutsche Forschungsgemeinschaft HA2686/15-1).

1. D. Pareyson, C. Marchesi, Diagnosis, natural history, and management of Charcot-Marie-Tooth disease. *Lancet Neurol.* **8**, 654–667 (2009).
2. L. Gutmann, M. Shy, Update on charcot-marie-tooth disease. *Curr. Opin. Neurol.* **28**, 462–467 (2015).
3. A. M. Rossor, P. J. Tomaselli, M. M. Reilly, Recent advances in the genetic neuropathies. *Curr. Opin. Neurol.* **29**, 537–548 (2016).
4. S. C. Previtali, A. Quattrini, A. Bolino, Charcot-Marie-Tooth type 4B demyelinating neuropathy: Deciphering the role of MTMR phosphatases. *Expert Rev. Mol. Med.* **9**, 1–16 (2007).
5. D. Pareyson *et al.*, A multicenter retrospective study of charcot-marie-tooth disease type 4B (CMT4B) associated with mutations in myotubularin-related proteins (MTMRs). *Ann. Neurol.* **86**, 55–67 (2019).
6. A. Bolino *et al.*, Charcot-Marie-Tooth type 4B is caused by mutations in the gene encoding myotubularin-related protein-2. *Nat. Genet.* **25**, 17–19 (2000).
7. H. Azzedine *et al.*, Mutations in MTMR13, a new pseudophosphatase homologue of MTMR2 and Sbf1, in two families with an autosomal recessive demyelinating form of Charcot-Marie-Tooth disease associated with early-onset glaucoma. *Am. J. Hum. Genet.* **72**, 1141–1153 (2003).
8. J. Senderek *et al.*, Mutation of the SBF2 gene, encoding a novel member of the myotubularin family, in Charcot-Marie-Tooth neuropathy type 4B2/11p15. *Hum. Mol. Genet.* **12**, 349–356 (2003).
9. K. Nakhro *et al.*, SET binding factor 1 (SBF1) mutation causes Charcot-Marie-Tooth disease type 4B3. *Neurology* **81**, 165–173 (2013).
10. K. Hnia, I. Vaccari, A. Bolino, J. Laporte, Myotubularin phosphoinositide phosphatases: Cellular functions and disease pathophysiology. *Trends Mol. Med.* **18**, 317–327 (2012).
11. M. A. Raess, S. Friant, B. S. Cowling, J. Laporte, WANTED - Dead or alive: Myotubularins, a large disease-associated protein family. *Adv. Biol. Regul.* **63**, 49–58 (2017).
12. G. Di Paolo, P. De Camilli, Phosphoinositides in cell regulation and membrane dynamics. *Nature* **443**, 651–657 (2006).
13. P. Berger, S. Bonneick, S. Willi, M. Wymann, U. Suter, Loss of phosphatase activity in myotubularin-related protein 2 is associated with Charcot-Marie-Tooth disease type 4B1. *Hum. Mol. Genet.* **11**, 1569–1579 (2002).
14. P. Berger, C. Schaffitzel, I. Berger, N. Ban, U. Suter, Membrane association of myotubularin-related protein 2 is mediated by a pleckstrin homology-GRAM domain and a coiled-coil dimerization module. *Proc. Natl. Acad. Sci. U.S.A.* **100**, 12177–12182 (2003).
15. M. A. Raess *et al.*, Expression of the neuropathy-associated MTMR2 gene rescues MTM1-associated myopathy. *Hum. Mol. Genet.* **26**, 3736–3748 (2017).
16. P. Berger *et al.*, Multi-level regulation of myotubularin-related protein-2 phosphatase activity by myotubularin-related protein-13/set-binding factor-2. *Hum. Mol. Genet.* **15**, 569–579 (2006).
17. F. L. Robinson, J. E. Dixon, The phosphoinositide-3-phosphatase MTMR2 associates with MTMR13, a membrane-associated pseudophosphatase also mutated in type 4B Charcot-Marie-Tooth disease. *J. Biol. Chem.* **280**, 31699–31707 (2005).

18. I. Vaccari *et al*., Genetic interaction between MTMR2 and FIG4 phospholipid phosphatases involved in Charcot-Marie-Tooth neuropathies. *PLoS Genet.* **7**, e1002319 (2011).
19. L. Sawade *et al*., Rab35-regulated lipid turnover by myotubularins represses mTORC1 activity and controls myelin growth. *Nat. Commun.* **11**, 2835 (2020).
20. X. Cai *et al*., PIKfyve, a class III PI kinase, is the target of the small molecular IL-12/IL-23 inhibitor apilimod and a player in Toll-like receptor signaling. *Chem. Biol.* **20**, 912–921 (2013).
21. A. Bolis *et al*., Dlg1, Sec8, and Mtmr2 regulate membrane homeostasis in Schwann cell myelination. *J. Neurosci.* **29**, 8858–8870 (2009).
22. C. Taveggia, A. Bolino, DRG neuron/schwann cells myelinating cocultures. *Methods Mol. Biol.* **1791**, 115–129 (2018).
23. A. L. Marat, V. Haucke, Phosphatidylinositol 3-phosphates-at the interface between cell signalling and membrane traffic. *EMBO J.* **35**, 561–579 (2016).
24. J. Viaud *et al*., Phosphoinositides: Important lipids in the coordination of cell dynamics. *Biochimie* **125**, 250–258 (2016).
25. J. Hasegawa, B. S. Strunk, L. S. Weisman, PI5P and PI(3,5)P_2: Minor, but essential phosphoinositides. *Cell Struct. Funct.* **42**, 49–60 (2017).
26. D. Bridges *et al*., Phosphatidylinositol 3,5-bisphosphate plays a role in the activation and subcellular localization of mechanistic target of rapamycin 1. *Mol. Biol. Cell* **23**, 2955–2962 (2012).
27. G. Figlia, D. Gerber, U. Suter, Myelination and mTOR. *Glia* **66**, 693–707 (2018).
28. G. Figlia, C. Norrmén, J. A. Pereira, D. Gerber, U. Suter, Dual function of the PI3-K-Akt-mTORC1 axis in myelination of the peripheral nervous system. *eLife* **6**, e29241 (2017).
29. B. Beirowski, K. M. Wong, E. Babetto, J. Milbrandt, mTORC1 promotes proliferation of immature Schwann cells and myelin growth of differentiated Schwann cells. *Proc. Natl. Acad. Sci. U.S.A.* **114**, E4261–E4270 (2017).
30. S. Goebbels *et al*., Genetic disruption of Pten in a novel mouse model of tomaculous neuropathy. *EMBO Mol. Med.* **4**, 486–499 (2012).
31. E. Domènech-Estévez *et al*., Akt regulates axon wrapping and myelin sheath thickness in the PNS. *J. Neurosci.* **36**, 4506–4521 (2016).
32. S. Bonneick *et al*., An animal model for Charcot-Marie-Tooth disease type 4B1. *Hum. Mol. Genet.* **14**, 3685–3695 (2005).
33. F. L. Robinson, I. R. Niesman, K. K. Beiswenger, J. E. Dixon, Loss of the inactive myotubularin-related phosphatase Mtmr13 leads to a Charcot-Marie-Tooth 4B2-like peripheral neuropathy in mice. *Proc. Natl. Acad. Sci. U.S.A.* **105**, 4916–4921 (2008).
34. K. Tersar *et al*., Mtmr13/Sbf2-deficient mice: An animal model for CMT4B2. *Hum. Mol. Genet.* **16**, 2991–3001 (2007).
35. A. Bolis *et al*., Loss of Mtmr2 phosphatase in Schwann cells but not in motor neurons causes Charcot-Marie-Tooth type 4B1 neuropathy with myelin outfoldings. *J. Neurosci.* **25**, 8567–8577 (2005).
36. A. Bolino *et al*., Disruption of Mtmr2 produces CMT4B1-like neuropathy with myelin outfolding and impaired spermatogenesis. *J. Cell Biol.* **167**, 711–721 (2004).
37. N. Tricaud, Myelinating schwann cell polarity and mechanically-driven myelin sheath elongation. *Front. Cell. Neurosci.* **11**, 414 (2018).
38. J. L. Salzer, Polarized domains of myelinated axons. *Neuron* **40**, 297–318 (2003).
39. S. Poliak, S. Matlis, C. Ullmer, S. S. Scherer, E. Peles, Distinct claudins and associated PDZ proteins form different autotypic tight junctions in myelinating Schwann cells. *J. Cell Biol.* **159**, 361–372 (2002).
40. C. Perrin-Tricaud, U. Rutishauser, N. Tricaud, P120 catenin is required for thickening of Schwann cell myelin. *Mol. Cell. Neurosci.* **35**, 120–129 (2007).
41. K. A. Newell-Litwa, R. Horwitz, M. L. Lamers, Non-muscle myosin II in disease: Mechanisms and therapeutic opportunities. *Dis. Model. Mech.* **8**, 1495–1515 (2015).
42. T. R. Arnold, R. E. Stephenson, A. L. Miller, Rho GTPases and actomyosin: Partners in regulating epithelial cell-cell junction structure and function. *Exp. Cell Res.* **358**, 20–30 (2017).
43. Y. Hara, Contraction and elongation: Mechanics underlying cell boundary deformations in epithelial tissue. *Dev. Growth Differ.* **59**, 340–350 (2017).
44. B. Beirowski *et al*., Sir-two-homolog 2 (Sirt2) modulates peripheral myelination through polarity protein Par-3/atypical protein kinase C (aPKC) signaling. *Proc. Natl. Acad. Sci. U.S.A.* **108**, E952–E961 (2011).
45. N. Golan *et al*., Genetic deletion of Cadm4 results in myelin abnormalities resembling Charcot-Marie-Tooth neuropathy. *J. Neurosci.* **33**, 10950–10961 (2013).
46. M. Horn *et al*., Myelin is dependent on the Charcot-Marie-Tooth Type 4H disease culprit protein FRABIN/FGD4 in Schwann cells. *Brain* **135**, 3567–3583 (2012).
47. L. Guo, C. Moon, Y. Zheng, N. Ratner, Cdc42 regulates Schwann cell radial sorting and myelin sheath folding through NF2/merlin-dependent and independent signaling. *Glia* **61**, 1906–1921 (2013).
48. N. Novak *et al*., N-WASP is required for membrane wrapping and myelination by Schwann cells. *J. Cell Biol.* **192**, 243–250 (2011).
49. J. B. Zuchero *et al*., CNS myelin wrapping is driven by actin disassembly. *Dev. Cell* **34**, 152–167 (2015).
50. S. Nawaz *et al*., Actin filament turnover drives leading edge growth during myelin sheath formation in the central nervous system. *Dev. Cell* **34**, 139–151 (2015).
51. P. Devreotes, A. R. Horwitz, Signaling networks that regulate cell migration. *Cold Spring Harb. Perspect. Biol.* **7**, a005959 (2015).
52. C. V. Melendez-Vasquez, S. Einheber, J. L. Salzer, Rho kinase regulates schwann cell myelination and formation of associated axonal domains. *J. Neurosci.* **24**, 3953–3963 (2004).
53. H. Wang, A. Tewari, S. Einheber, J. L. Salzer, C. V. Melendez-Vasquez, Myosin II has distinct functions in PNS and CNS myelin sheath formation. *J. Cell Biol.* **182**, 1171–1184 (2008).
54. K. Adlkofer *et al*., Heterozygous peripheral myelin protein 22-deficient mice are affected by a progressive demyelinating tomaculous neuropathy. *J. Neurosci.* **17**, 4662–4671 (1997).
55. J. A. Pereira *et al*., Integrin-linked kinase is required for radial sorting of axons and Schwann cell remyelination in the peripheral nervous system. *J. Cell Biol.* **185**, 147–161 (2009).
56. T. Chaya *et al*., Identification of a negative regulatory region for the exchange activity and characterization of T332I mutant of Rho guanine nucleotide exchange factor 10 (ARHGEF10). *J. Biol. Chem.* **286**, 29511–29520 (2011).
57. A. Roos *et al*., Inverted formin 2-related charcot-marie-tooth disease: Extension of the mutational spectrum and pathological findings in schwann cells and axons. *J. Peripher. Nerv. Syst.* **20**, 52–59 (2015).
58. T. Proikas-Cezanne, Z. Takacs, P. Dönnes, O. Kohlbacher, WIPI proteins: Essential PtdIns3P effectors at the nascent autophagosome. *J. Cell Sci.* **128**, 207–217 (2015).
59. B. Catimel *et al*., The PI(3,5)P2 and PI(4,5)P2 interactomes. *J. Proteome Res.* **7**, 5295–5313 (2008).
60. P. Gulhati *et al*., mTORC1 and mTORC2 regulate EMT, motility, and metastasis of colorectal cancer via RhoA and Rac1 signaling pathways. *Cancer Res.* **71**, 3246–3256 (2011).
61. L. Liu *et al*., Rapamycin inhibits cell motility by suppression of mTOR-mediated S6K1 and 4E-BP1 pathways. *Oncogene* **25**, 7029–7040 (2006).
62. D. D. Sarbassov *et al*., Rictor, a novel binding partner of mTOR, defines a rapamycin-insensitive and raptor-independent pathway that regulates the cytoskeleton. *Curr. Biol.* **14**, 1296–1302 (2004).
63. L. Liu *et al*., Rapamycin inhibits cytoskeleton reorganization and cell motility by suppressing RhoA expression and activity. *J. Biol. Chem.* **285**, 38362–38373 (2010).
64. L. Liu, S. Das, W. Losert, C. A. Parent, mTORC2 regulates neutrophil chemotaxis in a cAMP- and RhoA-dependent fashion. *Dev. Cell* **19**, 845–857 (2010).
65. Q. Venot *et al*., Targeted therapy in patients with PIK3CA-related overgrowth syndrome. *Nature* **558**, 540–546 (2018).
66. S. Gayle *et al*., Identification of apilimod as a first-in-class PIKfyve kinase inhibitor for treatment of B-cell non-Hodgkin lymphoma. *Blood* **129**, 1768–1778 (2017).
67. B. Payrastre, Phosphoinositides: Lipid kinases and phosphatases. *Methods Mol. Biol.* **273**, 201–212 (2004).